# FULLY CONSTRAINED OBLIQUE PROJECTION APPROACH TO MIXED PIXEL LINEAR UNMIXING

Mingyi He*, Shaohui Mei

School of Electronics and Information, Northwestern Polytechnical University,
Shaanxi Key Laboratory of Information Acquisition and Processing,
P.O. Box 612, Northwestern Polytechnical University, Xi'an 710072, China
E-mail: myhe@nwpu.edu.cn, meishaohui@gmail.com

**Commission VII, WG VII/4**

**KEY WORDS:** Hyperspectral, Multispectral, Sub-pixel classification, Processing, Recognition, Detection, Image

**ABSTRACT:**

Mixed pixels, which are inevitable in remote sensing images, often result in a lot of limitations in their applications. A novel approach for mixed pixel's fully constrained unmixing, Fully Constrained Oblique Subspace Projection (FCOBSP) Linear Unmixing algorithm, is proposed to handle this problem. The Oblique Subspace Projection, in which the signal space is oblique to the background space, is introduced to the settlement of the Linear Mixture Model (LMM). The abundance of constitutional spectral signature can be obtained through projecting the mixed pixel to the spectral signature subspace. One of the two well-known constraints of LMM, namely the non-negative constraint, is met by projecting mixed pixels to continually modified background space. The other constraint, namely the sum-to-one constraint, is embedded into the LMM to realize fully constrained linear unmixing. The performance of the proposed algorithm is evaluated by synthetic multispectral pixels decomposition. Compared with the popular Fully Constrained Least Square unmixing (FCLS) algorithm and Oblique Subspace Projection (OBSP), in terms of both RMSE and correlation coefficient with the real abundance, the proposed algorithm achieves significant improvement over these algorithms in spite of a little more time cost. The proposed algorithm has been used to handle the practical classification problems which dealing with the real multispectral and hyperspectral data, and the decomposition results show that the objects are well separated.

## 1. INTRODUCTION

Multispectral/hyperspectral remote sensing with characteristic of detailed spectral information has been widely utilized in many different areas such as land resource management, investigation of the forest vegetation, cultural relic protection, and so on (A. J. Tatem, 2003; Jiangtao, 2000; Gene, 2000; Mingyi He, 2007; Rui Huang and Mingyi He, 2005). Since the area that one pixel covers in a multispectral and/or hyperspectral image is usually pretty large (about 900 $m^2$ for NASA Landsat or 1.2 $km^2$ for NOAA-7) (Jun-Hua, 2004), one pixel usually contains more than one surface component, which often results in a mixture of these surface components. The mixed pixel problem not only influences the precision of object recognition and classification, but also becomes an obstacle to quantitative analysis of remote sensing images. This problem can be tackled by precisely obtaining the percentage of the objects contained in the mixed pixel. In fact, the exact decomposition of mixed pixels is of great importance in the field of sub-pixel classification of multispectral and hyperspectral remote sensing image as well as detection and identification of ground objects (Bin, 2005).

Charles Ichoku summarized the mixed pixel model into the following five types (Charles, 1996): the Linear Mixture Model (LMM), the Probabilistic Model, the Geometric Model, the Stochastic Geometric Model and the Fuzzy Model, in which the LMM is well known for its simple structure and clear physical meaning. Many mixed pixel unmixing algorithms based on the LMM have been applied to practical application, in which the least square algorithm is one of the most popular algorithms. Zhu Shulong used the least square method to solve the linear mixed model for mixed-pixel image classification (Zhu, 1995). Daniel Reinz etc. raised fully constrained least square unmixing algorithm to solve the minus abundance problem for material quantification (Daniel, 1999; Daniel, 2001). Recently, subspace projection has been introduced to the mixed pixel unmixing problem. The orthogonal subspace projection (OSP) method projects the signal to the space which is orthogonal to the background space to obtain the signal component by removing the background spectral component. Harsanyi and Chein-I etc. applied the OSP to hyperspectral image classification, dimension reduction and feature extraction, respectively (J. C. Harsanyi, 1994; Chein-I, 2005). The oblique subspace projection (OBSP) method, in which the desired signal subspace and the background subspace are oblique to each other for enhancing the desired signal as well as removing the background interference as much as possible, has been widely used in narrowband array processing, narrowband spectrum analysis, and so on (Richard, 1994). Chein-I etc. has already used OBSP algorithm to the mixed pixel classification (Chein-I, 1998). However, when using the OBSP to decompose the mixed pixel, the decomposition abundances can not meet the required two constraints imposed on LMM, namely non-negative and sum-to-one constraints, resultantly which can not be applied to the quantitative analysis of remote sensing. In this paper, a fully constrained oblique subspace projection mixed

* Corresponding author.

pixel unmixing algorithm is proposed to solve this problem. The minus abundance problem is conquered by modifying the endmember space to represent the constitution of the mixed pixel accurately. Experiments on synthetic spectral data, multispectral data and hyperspectral data are conducted separately to validate the algorithm.

## 2. LINEAR MIXTURE MODEL

The sketch map of the satellite remote sensing is shown in Figure 1. Due to the spatial resolution limitation, mixed pixel which contains energy reflected from more than one type of target in the remote sensing image are widely present. The mixed pixel is the consequence of many ground objects appearing in different proportions. In the LMM, the spectral response of mixed pixel is assumed to be the linear combination of the constitutional pure ground objects' signature and their ratios respectively. Generally, the pure ground objects contained in the mixed pixel is known as the endmember, while the corresponding ratio is known as the abundance. Therefore, the spectral reflection value of mixed pixel is the linearly weighted sum of spectral signature reflected from the inhomogeneous materials.

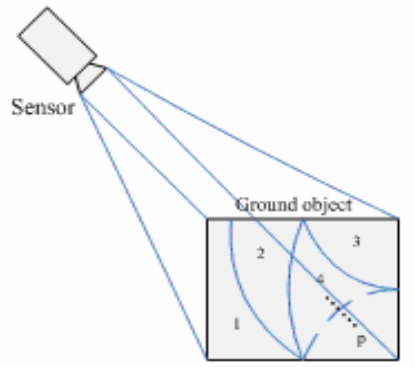


Figure 1. The sketch map of the satellite remote sensing

Let $\boldsymbol{r}=(r_1,r_2,\cdots,r_b)^{\mathrm{T}}$ be the mixed pixel vector in the multispectral/hyperspectral remote sensing image. Let matrix $M=(\boldsymbol{m}_1,\boldsymbol{m}_2,\cdots,\boldsymbol{m}_p)$ be the endmember matrix, where $\boldsymbol{m}_j=(m_{1j},m_{2j},\cdots,m_{bj})^T$ $(j=1,2,\cdots,p)$ is the *j*-th endmember of the mixed pixel, *b* is the band number, and *p* is the number of endmember contained in the mixed pixel. Let $\boldsymbol{\alpha}=(\alpha_1,\alpha_2,\cdots,\alpha_p)^T$ be the corresponding abundance vector, where $a_j$ is the abundance of the *j*-th endmember in the mixed pixel. Based on the linear mixing theory mentioned above the spectral signature of a mixed pixel can be represented by the linear regression model as follows:

$$\boldsymbol{r}=M\boldsymbol{\alpha}+\boldsymbol{n}=\sum_{j=1}^{p}m_j\alpha_j+\boldsymbol{n} \tag{1}$$

where $\boldsymbol{n}$ is a $b\times1$ column vector representing an additive white Gaussian noise with zero mean and variance $\sigma^2 I$, and $I$ is the $b\times b$ identity matrix.

Generally, the sum-to-one constraint and the non-negative constraint must be imposed in the expression to provide the LMM with adequate physical meaning, which can be expressed as follows:

$$\sum_{j=1}^{p}\alpha_j=1 \tag{2}$$

$$\alpha_j\geq0\quad j=1,2,\cdots,p \tag{3}$$

## 3. THE OBLIQUE SUBSPACE PROJECTION

Let $\mathbb{F}$ and $\mathbb{S}$ be two subspaces of the *n*-dimension space $C^{\mathrm{n}}$. The transformation which projects arbitrary $\boldsymbol{x}$ contained in $C^{\mathrm{n}}$ to the subspace $\mathbb{F}$ along $\mathbb{S}$ is known as the projection along $\mathbb{S}$ to $\mathbb{F}$. Let $P_{\mathbb{F},S}$ be the projection operator along $\mathbb{S}$ to $\mathbb{F}$, so we have

$$P_{\mathbb{F},\mathbb{S}}(\boldsymbol{x})=\boldsymbol{y}\quad \boldsymbol{x}\in\mathbb{F},\boldsymbol{y}\in\mathbb{S} \tag{4}$$

Let *P* be the projection matrix of the projection operator $P_{L,M}$, so *P* must be idempotent, which means it must equal to its own square:

$$P^2=P \tag{5}$$

If the subspace $\mathbb{F}$ is orthogonal to the subspace $\mathbb{S}$, the projection $P_{L,M}$ is known as orthogonal projection. As for the oblique projection, the subspace $\mathbb{F}$ is oblique to the subspace $\mathbb{S}$. In other words, $\mathbb{F}$ is disjoint to $\mathbb{S}$. Based on the projection theory aforementioned, for an oblique projector $E_{HS}$ whose range is $\langle H\rangle$ and whose null space contains $\langle S\rangle$, we have

$$\begin{cases}E_{HS}\bullet\mathrm{H}=\mathrm{H}\\ E_{HS}\bullet\mathrm{S}=0\\ E_{HS}^2=E_{HS}\end{cases} \tag{6}$$

The geometric figure of projector $E_{HS}$ is shown in Figure 2.

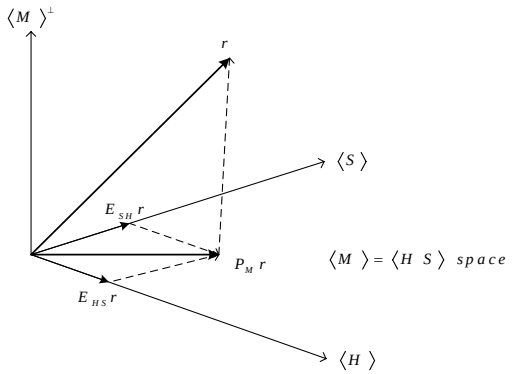


Figure 2. The geometric figure of oblique projection

Assume that *H* is a complex matrix of size $n\times m$ having full column rank and, likewise, assume that *S* is a complex matrix of size $n\times t$ having full column rank. Further assume that $\langle H\rangle$ and $\langle S\rangle$ is disjoint, which requires $m+t\leq n$. For an oblique projector $E_{HS}$ whose range is $\langle H\rangle$ and whose null space contains $\langle S\rangle$, we have (Richard, 1994)

$$\mathrm{E_{HS}}=(\mathrm{H}\ 0)\begin{pmatrix}\mathrm{H^HH} & \mathrm{H^HS}\\ \mathrm{S^HH} & \mathrm{S^HS}\end{pmatrix}^{-1}\begin{pmatrix}\mathrm{H^H}\\ \mathrm{S^H}\end{pmatrix} \tag{7}$$

Obviously, $E_{HS}$ meets formula (6), and $E_{HS}$ is an oblique projection matrix.

Equation (7) for the oblique projector $E_{HS}$ can be simplified to either of the following:

$$E_{HS}=H\left(H^HP_S^{\perp}H\right)^{-1}H^HP_S^{\perp} \tag{8a}$$

$$E_{HS} = P_H \left( I - S \left( S^H P_H^{\perp} S \right)^{-1} S^H P_H^{\perp} \right) \tag{8b}$$

where,

$$P_{\mathrm{H}}^{\perp} = I - P_{\mathrm{H}}, \quad P_{\mathrm{H}} = H(H^{\mathrm{H}}H)^{-1}H^{\mathrm{H}} \tag{9}$$

$$P_S^{\perp} = I - P_S, \quad P_S = S(S^H S)^{-1} S^H \tag{10}$$

$P_H$ is the orthogonal projector whose range is $\langle H \rangle$ while $P_H^{\perp}$ is the orthogonal projector whose range is $\langle H \rangle^{\perp}$. Similarly, $P_S$ is the orthogonal projector whose range is $\langle S \rangle$ and $P_S^{\perp}$ is the orthogonal projector whose range is $\langle S \rangle^{\perp}$.

## 4. THE OBLIQUE SUBSPACE PROJECTION BASED UNMIXING OF MIXED PIXEL

In the space constituted by the endmember $\langle M \rangle$, let endmember $\langle H_j \rangle = \langle m_j \rangle (j = 1, 2, \cdots, p)$ be the signal's spectral space which only contains the concerned spectral signature and other endmember $\langle S_j \rangle = \langle m_1, \cdots, m_i, \cdots, m_p \rangle \ (i = 1, 2, \cdots, p; i \neq j)$ be the background space. Therefore we have,

$$\langle M \rangle = \langle H_j \ S_j \rangle \quad j = 1, 2, \cdots p \tag{11}$$

Let $E_j$ be the oblique projector whose range is $\langle H_j \rangle$ and null space contains $\langle S_j \rangle$. It can be obtained by formula (8a) and (8b). Applying oblique projector $E_j$ to the LMM of mixed pixel defined by formula (1) yields

$$\begin{aligned} o_j &= E_j \boldsymbol{r} \\ &= E_j M \boldsymbol{\alpha} + E_j \boldsymbol{n} \\ &= E_j \left( H_j \ S_j \right) \boldsymbol{\alpha} + E_j \boldsymbol{n} \\ &= E_j H_j \alpha_j + E_j \boldsymbol{n} \\ &= H_j \alpha_j + E_j \boldsymbol{n} \end{aligned} \tag{12}$$

where $o_j$ is the oblique projection of the mixed pixel to the signal space $\langle H_j \rangle$, which is denoted as the oblique projection of endmember $H_j$.

Regardless of the influence of the Gaussian noise, the oblique projection of the endmember $H_j$ is given by

$$o_j = H_j \alpha_j \tag{13}$$

By using of the generalized pseudo matrix of $H_j$, the abundance of endmember $H_j$ in the mixed pixel $\boldsymbol{r}$ can be derived by

$$\begin{aligned} \alpha_j &= \left( H_j^T H_j \right)^{-1} H_j^T o_j \\ &= \left( H_j^T H_j \right)^{-1} H_j^T E_j \boldsymbol{r} \\ &= \left( H_j^T P_{S_j}^{\perp} H_j \right)^{-1} H_j^T P_{S_j}^{\perp} \boldsymbol{r} \end{aligned} \tag{14}$$

## 5. FULLY CONSTRAINED OBLIQUE SUBSPACE PROJECTION TO MIXED PIXEL LINEAR UNMIXING

Taking the two constraints of the mixed pixel model into account during the process of the mixed pixel oblique projection unmixing, the fully constrained decomposition can be reached.

### 5.1 The Sum-to-one Constraint

For analysis convenience, denote $\delta_0 = \alpha_1 + \alpha_2 + \cdots + \alpha_p$, equation (1) is modified as:

$$\begin{pmatrix} r_1 \\ \vdots \\ r_b \\ \delta_0 \end{pmatrix} = \begin{pmatrix} m_{11} & \cdots & m_{1p} \\ \vdots & \ddots & \vdots \\ m_{b1} & \cdots & m_{bp} \\ 1 & \cdots & 1 \end{pmatrix} \begin{pmatrix} \alpha_1 \\ \vdots \\ \alpha_p \end{pmatrix} + \begin{pmatrix} n_1 \\ \vdots \\ n_p \\ 0 \end{pmatrix} \tag{15}$$

Considering the sum-to-one constraint, the LMM can be further modified as follows:

$$\begin{pmatrix} r_1 \\ \vdots \\ r_b \\ \delta \end{pmatrix} = \begin{pmatrix} m_{11} & \cdots & m_{1p} \\ \vdots & \ddots & \vdots \\ m_{b1} & \cdots & m_{bp} \\ \delta & \cdots & \delta \end{pmatrix} \begin{pmatrix} \alpha_1 \\ \vdots \\ \alpha_p \end{pmatrix} + \begin{pmatrix} n_1 \\ \vdots \\ n_p \\ 0 \end{pmatrix} \tag{16}$$

where $\delta$ is the trade-off between the Sum-to-one constraint and the LMM. Applying the Oblique Projection Approach to the modified LMM defined by formula (16), the abundances could meet the sum-to-one constraint.

### 5.2 The Non-negative Constraint

As all the endmember of the remote image is usually not totally contained in one certain pixel, using the oblique projection to decompose the mixed pixel based on the assumption that all the endmember are contained in the pixel, may produce negative projection, which makes the abundance less than zero and can not meet the non-negative constraint of the LMM. Accordingly, it is crucial to know the precise endmember constitution of one certain mixed pixel. Based on the iterative method (Daniel, 2000), the background space can be continually modified by wiping off the spectral signature which corresponds to the largest minus projection from the endmember space in order to get the precise constitution of the pixel. The abundance can be achieved by repeating the iterative process until all the abundances meet the non-negative constraint. The detail algorithm is as follows:

**Step 1:** Calculate the abundance of each spectral signature in the mixed pixel by formula (14).

**Step 2:** If all the abundance of the spectral signature contained in the mixed pixel is nonnegative, which means $\alpha_j \geq 0 (j = 1, 2, \cdots, p)$, the precise endmember constitution is obtained and the correct decomposition result is determined. Otherwise, turn to step 3 to modify the endmember constitution.

**Step 3:** Find out the biggest minus abundance, and let it be 0. Then modify the endmember constitution by wiping off the corresponding spectral signature from the endmember matrix to get the new endmember matrix composed by the residual spectral signature. Turn to step 1 and use the new endmember matrix to decompose again.

The proposed fully constrained oblique projection (FCOBSP) algorithm requires a maximum of $p$-1 iterations and terminates when the correct endmember constitution is obtained.

## 6. EXPERIMENTS

In this section, several experiments are conducted on synthetic multispectral pixels, Landsat-7 multispectral images, and hyperspectral images separately to validate the proposed FCOBSP algorithm.

### 6.1 Experiments on Synthetic Multispectral Data

The typical signature obtained by Landsat-7 is used as endmember to simulate multispectral mixed pixels to evaluate the performance of the proposed Fully Constrained Oblique Subspace Projection (FCOBSP) Linear Unmixing algorithm against the popular Fully constrained least square (FCLS) algorithm (Daniel, 2001b) and Oblique subspace projection (OBSP) algorithm (known as OBC of Chein-I, 1998b). The reflected spectrum of four ground objects including building, swamp, water, and road with spectral range 529-920nm shown in Figure 3, are adopted. Therefore, the endmember matrix $M=(\boldsymbol{m}_1,\boldsymbol{m}_2,\boldsymbol{m}_3,\boldsymbol{m}_4)$ consisted of four spectral signatures with abundance fractions given by $\boldsymbol{\alpha}=(\alpha_1,\alpha_2,\alpha_3,\alpha_4)^{\mathrm{T}}$. The multi-spectral pixel simulation method is the same with it considering in Daniel's paper (Daniel, 1999). When simulating the multispectral pixel, we started the first pixel vector with 100% building and 0% other ground objects, and then began to decrease 1% building every pixel vector until the 100th pixel vector which contained 1% building. Correspondingly, the other components of swamp, water, and road totally increase by the increment of 1%, where the increment ratio among them is 5:3:2, which means the swamp increases from 0 to 50% by the increment of 0.5%, the water increases from 0 to 30% by the increment of 0.3%, and the swamp increases from 0 to 20% by the increment of 0.2%. White Gaussian noise is added to each pixel vector to achieve a 50:l signal-to-noise ratio (J. C. Harsanyi, 1994).

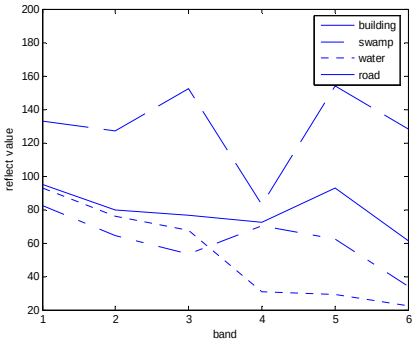


Figure 3. Four ground objects typical spectrum of Landsat-7

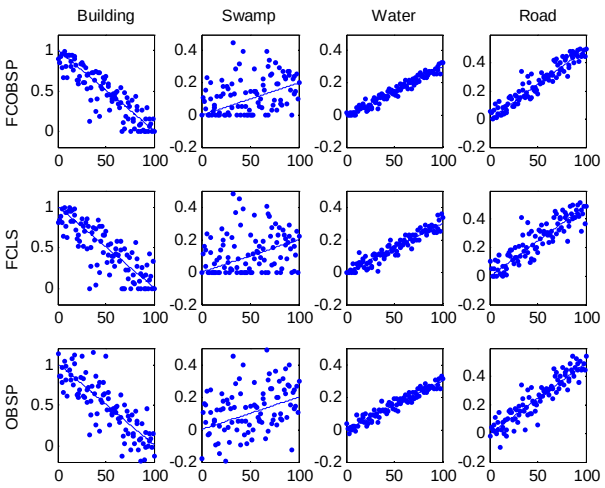


Figure 4. The decomposition results of the three algorithms (SNR=10dB)

Figure 4 shows the simulated multispectral pixel decomposition results of applying the FCOBSP, FCLS, and OBSP algorithms at the SNR level of 10dB respectively. It should be noted that the outputs in Fig.4 were plotted in real ranges of abundance, e.g. [0,1]. The comparisons between FCOBSP and other methods in the aspects of the root-mean-square error, correlation coefficient, and time cost are shown in Table 1. The root mean square error (RMSE) and correlation coefficient between estimated abundance and real abundance are defined by formula (17) and (18) respectively.

$$Cor=(\sum_{i=1}^{p}(\alpha_{\text{estimate}}\times\alpha_{\text{real}}))/\sqrt{\sum_{i=1}^{p}\alpha_{\text{estimate}}^2}\sqrt{\sum_{i=1}^{p}\alpha_{\text{real}}^2} \quad (17)$$

$$RMSE=\sum_{i=1}^{p}(\alpha_{\text{estimate}}-\alpha_{\text{real}})^2 \quad (18)$$

The computer with Pentium 4 at 3.20GHz CPU and 512M RAM is taken to measure the time cost.

| | Root Mean Square Error | Correlation Coefficient | Time Cost /s |
|---|---|---|---|
| FCOBSP | **0.0897** | **0.9038** | 0.047 |
| FCLS | 0.1061 | 0.8849 | 0.031 |
| OBSP | 0.1480 | 0.8256 | **0.016** |

Table 1. The performance of the three algorithms

It can be deduced from Table 1 that:

(1) The FCOBSP algorithm, which gets the least root mean square error and the largest correlation coefficients with the real abundance fractions, is better than the other two algorithms in spite of a little more time cost. Although the OBSP algorithm spend less time than FCOBSP, it may lead to minus abundance fractions, which may not meet the linear mixed model and can not be applied in the quantitative analysis of remote sensing images. The FCOBSP algorithm confines the fraction of abundance to [0,1], and the sum of those abundances is restricted to one to meet the LMM.

(2) Although the FCLS algorithm can also confine the abundance fractions to [0, 1], the FCOBSP possesses more accurate decomposition results in the aspects of the least root-mean-square error and the correlation coefficients with real results.

Figure 5 shows the correlation coefficients between the estimated abundance and the real simulated abundance at different noise level. Obviously, the decomposition results by using FCOBSP are more accurate than the other two algorithms especially when the SNR is low.

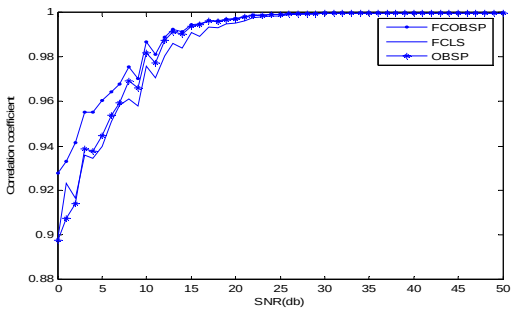


Figure 5. The decomposition correlation coefficient at different noise level

### 6.2 Experiments with Landsat-7 Multispectral Images

In this section, a real multispectral scene of Shenzhen area of China, collected by the Landsat-7 satellite, is adopted to show the performance of the proposed algorithm. The scene consists of 7 bands covering a spectral range 529-920nm. However, only bands from 1 to 5 together with band 7, the spatial resolution of which is 30m, are selected, for band 6 at a different spatial resolution is for other use. Figure 6 shows a Landsat-7 false colour image of this area, with the band 1 displayed as red, the

Figure 6. The false color image of Shenzhen

band 3 as green, and the band 5 as blue. Ground objects such as water, building, swamp, and road etc. are contained in this area. The experiment chooses 6 endmember whose spectral curves are shown in Figure 7 to apply to the FCOBSP algorithm. The decomposition results of the proposed algorithm, denoted by abundance gray image, are shown in Figure 8. In these images, pure black denotes that the percentage of a certain sort of object in this pixel is 0, while pure white denotes 1. Obviously, the proposed algorithm is successful in decomposing the Landsat-7 multispectral images into 6 ground objects.

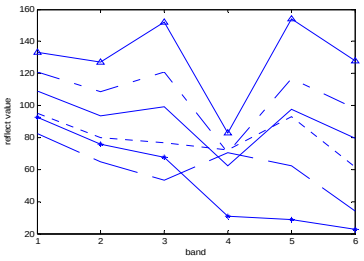


Figure 7. The typical spectral of Shenzhen

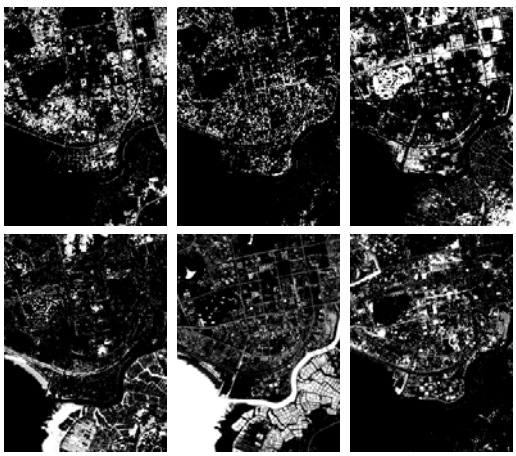

Figure 8. The decomposition result of Shenzhen

### 6.3 Experiments with Hyperspectral Images

In the final experiment, the proposed algorithm is applied to a hyperspectral scene of the Jasper Ridge area located in California of USA on Jul 18th, 2000. The scene consists of $512 \times 600$ pixels, each containing 60 bands covering the spectrum ranging from 441.0nm to 1320.8nm. The total 60 bands are selected. Figure 9 shows a false color image of this area, with the band 1displayed as red, the band 20 as green, and the band 30 as blue. As shown in Figure 10, this area mainly includes 5 kinds of typical ground objects: water, vegetation, and 3 kinds of soil (includes road). By using these 5 kinds of ground objects as endmember, the decomposition result of applying the proposed algorithm is shown in Figure 11. Based on the fractional gray images, the five ground objects are well separated.

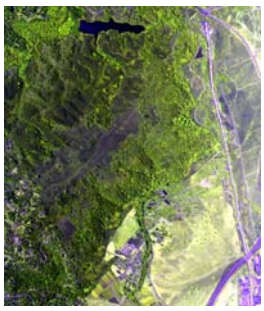

Figure 9. The false color image of Jasper Ridge

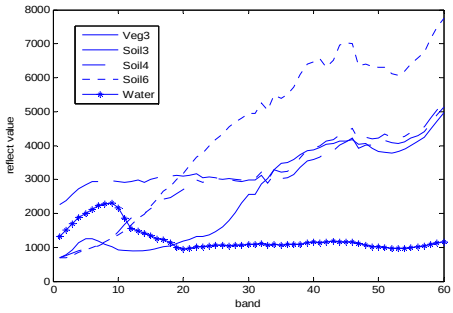


Figure 10. Typical spectrum of Jasper Ridge

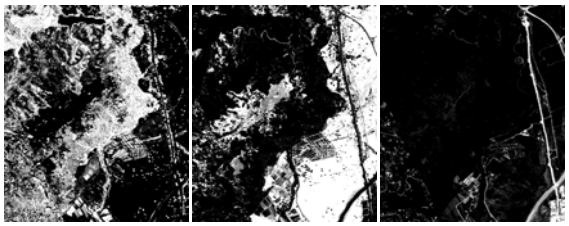

a. Veg 3 b. Soil 3 c. Soil 4

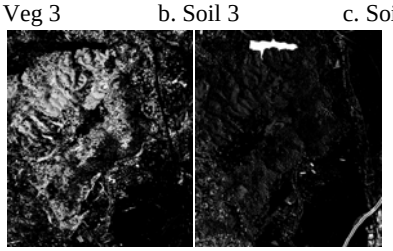

d. Soil 6 e. Water

Figure 11. The decomposition results of Jasper Ridge

## 7. CONCLUSION

In this paper, a novel approach for mixed pixel's fully constrained unmixing has been developed and demonstrated. The algorithm firstly uses the oblique projection to decompose the mixed pixel and then iterates to realize the fully constrained decomposition. The oblique projection, which projects signal to the subspace oblique to a low rank subspace, can eliminate the noise as well as enhance the desired signal as much as possible. Based on the LMM, the abundance of spectral signature can be obtained by using the oblique projection, which means projecting the pixel vector to the signal subspace which is oblique to the background and noise subspace. The FCOBSP algorithm adjusts the abundance to meet the constraints of the LMM by repetitiously projecting mixed pixel to continually modified background space. The synthetic experiment provides that, compared with the other popular mixed pixel unmixing algorithm such as OBSP and FCLS, the FCOBSP gets the least root mean square error and the largest correlation coefficients with the real abundance fractions, and is better than other algorithms although a slightly more time cost. The FCOBSP mixed pixel unmixing could be generalized to apply to wider applications dealing with multispectral and/or hyperspectral images.

## ACKNOWLEGEMENT

This work is supported by National Natural Science Foundation of China (project number 60572097 and key project number 60736007) and NPU fundamental research program.

## REFERENCES

A. J. Tatem, H. G. Lewis, P. M. Atkinson, M. S. Nixon, 2003. Increasing the spatial resolution of agricultural land cover maps using a Hopfield neural network. *International Journal of Geographical Information Science*, 17(7), pp.647-672.

Bin Wang, Hao Zhou, Liming Zhang, 2005. Blind Decomposition of Mixed Pixels Using Constrained Non-Negative Matrix Factorization. In: *IEEE 2005 International Geoscience and Remote Sensing Symposium*, 6, pp. 3757-3760.

Charles Ichoku, Arnon Karnieli, 1996. A review of mixture modeling techniques for sub-pixel land cover estimation. *Remote Sensing Reviews*, 13, pp. 161-186.

Chein-I Chang, 2005. Orthogonal Subspace Projection (OSP) Revisited: A Comprehensive Study and Analysis. *IEEE Transactions on Geoscience and Remote sensing*, 43, pp. 502-518.

Chein-I Chang, Xiao-Li Zhao, Mark L. G. Althouse, Jeng Jong Pan, 1998. Least Squares Subspace Projection Approach to Mixed Pixel Classification for Hyperspectral Images. *IEEE Transactions on Geoscience and Remote Sensing*, 36, pp. 898-912.

Daniel Reinz, Chein-I Chang, Mark L.G. Althouse, 1999. Fully Constrained Least-Squares Based Linear Unmixing. In: *IEEE 1999 International Geoscience and Remote Sensing Symposium*. Hamburg, Germany, pp.1401-1403.

Daniel C. Heinz, Chein-I Chang, 2001. Fully Constrained Least Squares Linear Spectral Mixture Analysis Method for Material Quantification in Hyperspectral Imagery. *IEEE Transactions on Geoscience and Remote sensing*, 39, pp. 529-545.

Gene A. Ware, 2000. Multispectral Analysis of Ancient Maya Pigments: Implications for the Naj Tunich Corpus. *IEEE 2000 International Geoscience and Remote Sensing Symposium*, 6, pp. 2489-2491.

J. C. Harsanyi, C.-I Chang, 1994. Hyperspectral image classification and dimensionality reduction: An orthogonal subspace projection. *IEEE Transactions on Geoscience and Remote sensing*, 32, pp. 779-785.

Jiangtao Lee, Yanmin Shuai, Qijiang Zhu, 2004. Using images combined with DEM in classifying forest vegetations. *IEEE 2004 International Geoscience and Remote Sensing Symposium*, 4, pp. 2362-2364.

Jun-Hua Han, De-Shuang Huang, Zhan-Li Sun, Yiu-ming Cheung, 2004. A Novel Mixed Pixels Unmixing Method for Multispectral Images. *Neural Networks*, 4, pp. 2541-2545.

Mingyi He, 2007. Advances in Signal and Image Processing for Hyperspectral Remote Sensing, Invited talk, *Proc of IEEE ICIEA'07*, May 23-25, 2007

Richard T. Behrens, Louis L. Scharf, 1994. Signal Processing Applications of Oblique Projection Operators. *IEEE Transactions on Signal Processing*, 42, pp. 1413-1424.

Rui Huang, Mingyi He, 2005. Band selection based on feature weighting for classification of hyperspectral data, *IEEE Geoscience and Remote Sensing Letters*, 2(2)

Zhu Shulong, 1995. The classification of Remotely--Sensed Images with Mixels. *Chinese Journal of Institute of Surveying and Mapping*, 12, pp. 276-278.